Heliyon 8 (2022) e08741

Contents lists available at ScienceDirect

Heliyon

journal homepage: www.cell.com/heliyon

Research article

Clinical and magnetic resonance imaging feature differences between solitary and multiple type Langerhans cell histiocytosis involving the craniofacial bone

Shu Matsushita [a,b,*], Taro Shimono [b], Tomohisa Okuma [a], Takeshi Inoue [c], Takao Manabe [a], Yukio Miki [b]

[a] Department of Diagnostic Radiology, Osaka City General Hospital, 2-13-22 Miyakojima-Honndori, Miyakojima-ku, Osaka 534-0021, Japan
[b] Department of Diagnostic and Interventional Radiology, Graduate School of Medicine, Osaka City University, 1-4-3 Asahi-machi, Abeno-ku, Osaka 545-8585, Japan
[c] Department of Pathology, Osaka City General Hospital, 2-13-22 Miyakojima-Honndori, Miyakojima-ku, Osaka 534-0021, Japan

HIGHLIGHTS

- Patient age at presentation was higher in the SLG than that in the MLG.
- The SLG showed more extensive bone marrow edema and enhancement than the MLG.
- Clinical and MRI features may help differentiate LCH manifestation types.

GRAPHICAL ABSTRACT

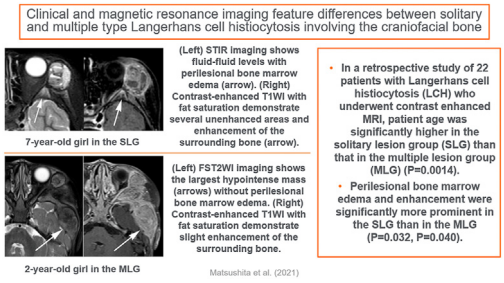

ARTICLE INFO

Keywords:
Langerhans cell histiocytosis
Craniofacial bone
Magnetic resonance imaging

ABSTRACT

Purpose: To investigate the clinical and contrast-enhanced magnetic resonance imaging (MRI) features of craniofacial bone Langerhans cell histiocytosis (LCH) and discuss the differences between a solitary lesion group (SLG) and multiple lesions group (MLG).

Method: This study included 22 consecutive patients with pathologically proven LCH who underwent contrast-enhanced MRI. The clinical data and MRI features were retrospectively assessed.

Results: The mean patient age was 5 years, and 15 patients were male. The frontal bone was the most frequently affected bone. Ten and 12 patients were classified into the SLG and the MLG, respectively. The following MRI features were observed in >50% cases: T1WI hyperintensity in 15 (68%) cases, T2WI hyperintensity in 16 (73%) cases, bulging sign in 18 (82%) cases, concentric or eccentric soft tissue mass formation in 13 (59%) cases, soft tissue edema in 16 (73%) cases, any grade of bone marrow edema in 16 (73%) cases, surrounding bone enhancement in 17 (77%) cases, and surrounding soft tissue enhancement in 16 (73%) cases. Patient age was significantly higher in the SLG than that in the MLG ($P = 0.0014$). Perilesional bone marrow edema and enhancement were significantly more prominent in the SLG than in the MLG ($P = 0.032$, $P = 0.040$).

Conclusions: Contrast-enhanced MRI showed additional significant findings of mainly the surrounding details. Older age, extensive bone marrow edema, and enhancement may indicate solitary-type LCH rather than multiple-type LCH. These differences may help distinguish between solitary- and multiple-type LCH, which have different treatment strategies.

* Corresponding author.
E-mail address: shumatsu@med.osaka-cu.ac.jp (S. Matsushita).

https://doi.org/10.1016/j.heliyon.2022.e08741
Received 15 September 2021; Received in revised form 17 November 2021; Accepted 7 January 2022

1. Introduction

Langerhans cell histiocytosis (LCH) is a multi-system disorder characterized by abnormal proliferation of histiocytic cells. This disease may affect any age group, but it mainly affects children aged <15 years [1]. There are several recognized manifestation types and categories based on the extent of the disease—single-system single-site (SS-s), single-system multifocal-site (SS-m, involvement of a single organ or system), and multi-system (MS, involvement of two or more organs). Patients with solitary (single)-type LCH have a good prognosis and usually require only local therapy or observation, whereas patients with multiple (multifocal and multi-system)-type LCH require chemotherapy [1].

Craniofacial bones are important regions not only because they are the most commonly affected site in patients with LCH [2] but also because they include central nervous system (CNS) risk bones such as the orbital, temporal, sphenoid, ethmoid, and mastoid bones. Patients with CNS risk bone lesions have a higher risk of developing diabetes insipidus and other CNS manifestations; therefore, chemotherapy is recommended even if the lesion is localized in these bones, except in the case of solitary LCH [3].

Since there is no specific biological marker of disease activity in LCH, whole-body examination is usually performed at initial diagnosis, and skeletal radiography is the gold standard. The use of other modalities such as whole-body bone scintigraphy, magnetic resonance imaging (MRI), and fluorodeoxyglucose-positron emission tomography have been discussed; however, there is currently no recommendation for them to be used as alternative imaging surveys [4, 5]. This is due to the fact that patients with LCH are mainly children, and sedation or general anesthesia is required for whole-body scans. In follow-up radiography, examination of the initially involved anatomic region should be limited to minimize the patient's exposure to ionizing radiation [4]. Although these initial and follow-up examinations cannot be waived, the difference in imaging appearance between manifestation types may contribute to the therapeutic strategy and interval employed in follow-up studies.

Table 2. Comparison of the clinical and imaging findings between the SLG and MLG.

	All (n = 22)	SLG (n = 10)	MLG (n = 12)	*P* value
Age at presentation (mean)	1-17 (5)	5-17 (9)	1-10 (2)	0.0014
Sex (male:female)	15:7	8:2	7:5	0.38
Hyperintense/isointense/hypointense on T1WI	15/7/0	8/2/0	7/5/0	0.38
Hyperintense/isointense/hypointense on T2WI	16/3/3	6/3/1	10/0/2	0.17
Hypointense rim (absent/partial/circumferential)	21/0/1	9/0/1	12/0/0	0.46
Necrotic or cystic part (yes/no)	11/11	6/4	5/7	0.67
FFL (yes/no)	5/17	4/6	1/11	0.14
Penumbra sign (yes/no)	5/17	4/6	1/11	0.14
Bulging (yes/no)	18/4	8/2	10/2	1
Budding (yes/no)	1/21	1/9	0/12	0.46
Soft tissue mass (absent/concentric/eccentric)	9/7/6	4/3/3	5/4/3	1
Soft tissue edema (yes/no)	16/6	8/2	8/4	0.65
Marrow edema (absent/grade 1/grade 2/grade 3)	6/9/3/4	1/4/1/4	5/5/2/0	0.032
Enhancement pattern (homogeneous/heterogeneous/rim-like)	9/11/2	4/4/2	5/7/0	0.39
Enhancement of surrounding bone (yes/no)	17/5	10/0	7/5	0.040
Enhancement of surrounding soft tissue (yes/no)	16/6	6/4	10/2	0.35
Meningeal enhancement (yes/no)	8/14	5/5	3/9	0.38

SLG, solitary lesion group; MLG, multiple lesion group; FFL, fluid-fluid level; WI, weighted imaging.

Table 1. Clinical characteristics of 22 cases of craniofacial LCH.

No.	Age	Sex	Affected bone	Manifestation type	Treatment	Details of manifestation
1	16	M	Rt. parietal	SS-s	Excision	
2	2	M	Frontal	SS-s	Excision	
3	10	M	Frontal	SS-s	Excision	
4	8	M	Occipital	SS-s	Excision	
5	17	M	Occipital	SS-s	Excision	
6	7	F	Occipital	SS-s	Excision	
7	5	M	Frontal	SS-s	Excision	
8	7	F	Lt. zygomatic	SS-s	Chemotherapy	
9	10	M	Occipital	SS-s	Excision	
10	15	M	Lt. parietal	SS-s	Excision	
11	3	M	Bilateral parietal, rt. temporal	SS-m	Chemotherapy	Co-exists with lt. femoral bone lesion
12	3	M	Frontal	SS-m	Chemotherapy	Post treatment recurrence (cervical vertebra and lt. femoral bone)
13	2	F	Rt. Temporal	SS-m	Chemotherapy	Post treatment recurrence (rt. rib)
14	2	M	Diffuse cranium	SS-m	Chemotherapy	Co-exists with rt. iliac bone lesion
15	10	M	Frontal	SS-m	Chemotherapy	Co-exists with lumbar vertebral lesion
16	1	F	Frontal	SS-m	Chemotherapy	Co-exists with rt. femoral bone lesion
17	3	M	Frontal	SS-m	Chemotherapy	Close recurrence in occipital bone after resection
18	4	M	Rt. mandibular ramus	SS-m	Chemotherapy	Co-exists with lt. rib and thoracic vertebral lesions
19	1	F	Rt. temporal	MS	Chemotherapy	Co-exists with rib, liver, and spleen lesions
20	2	F	Sphenoid, lt. temporal and frontal	MS	Chemotherapy	Co-exists with multiple bone lesions, lymph nodes, and central nervous system infiltration (diabetes insipidus)
21	1	F	Lt. temporal	MS	Chemotherapy	Co-exists with thyroid gland lesion
22	1	M	Bilateral temporal	MS	Chemotherapy	Co-exists with multiple bone, thyroid gland, thymus, and liver lesions

SS-s, single-system single-site; SS-m, single-system multifocal site; MS, multi-system; lt., left; rt., right.

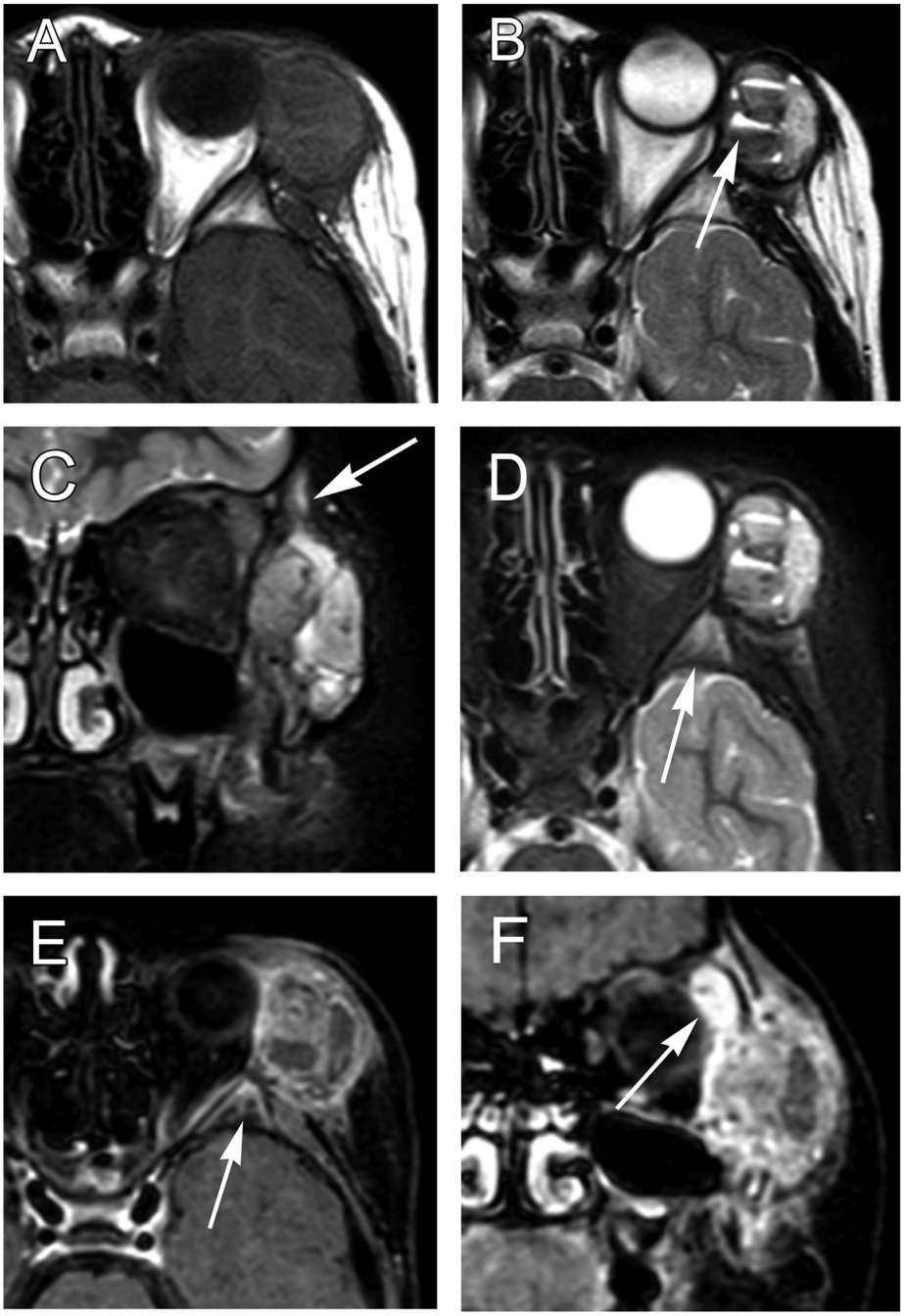

Figure 1. Single-system single-site-type left zygomatic bone LCH of a 7-year-old girl (case 8). (A) Axial T1WI demonstrates a slight hyperintense lesion in the lateral wall of the left orbit with a bulging sign making a concentric soft tissue mass. (B) Axial T2WI demonstrates a hyperintense multilocular mass with fluid-fluid levels (arrow). (C) and (D) Coronal and axial short-tau inversion recovery imaging shows soft tissue edema (C: arrow) with grade 1 bone marrow edema (D: arrow). (E) and (F) Axial and coronal contrast-enhanced T1WI with fat saturation demonstrate several unenhanced areas and enhancement of the surrounding bone and soft tissue (arrow). WI, weighted imaging.

To date, the largest radiographic and MRI review of pathologically proven LCH of the shoulder girdle, pelvis, and extremities included 85 cases [6]. However, the authors did not review the radiographic and MRI features of craniofacial LCH. Typical skeletal imaging features of craniofacial LCH have been described as lytic lesions with or without sequestrum on computed tomography, which show hyperintensity on T2-weighted imaging (WI) and variable signal intensity on T1WI, with variable enhancement after gadolinium-based contrast agent administration on MRI [7, 8]. D'Ambrosio et al. [7] documented a large series of craniofacial and intracranial LCH; however, they did not investigate the MRI findings of the internal and surrounding details, and the precise imaging features of contrast-enhanced T1WI were unclear because the number of patients was not reported. Furthermore, the differences in radiographic and MRI features between the SS-s, SS-m, and MS types of craniofacial LCH have not been investigated in previous studies.

The aim of this study was to investigate the clinical and MRI features, along with the internal and surrounding details, of craniofacial bone LCH using contrast-enhanced examination and discuss the differences between the solitary and multiple type of craniofacial bone LCH in a series of pathologically proven cases.

2. Materials and methods

2.1. Subjects

This retrospective study was approved by the institutional review board of our institution, and the requirement for obtaining written

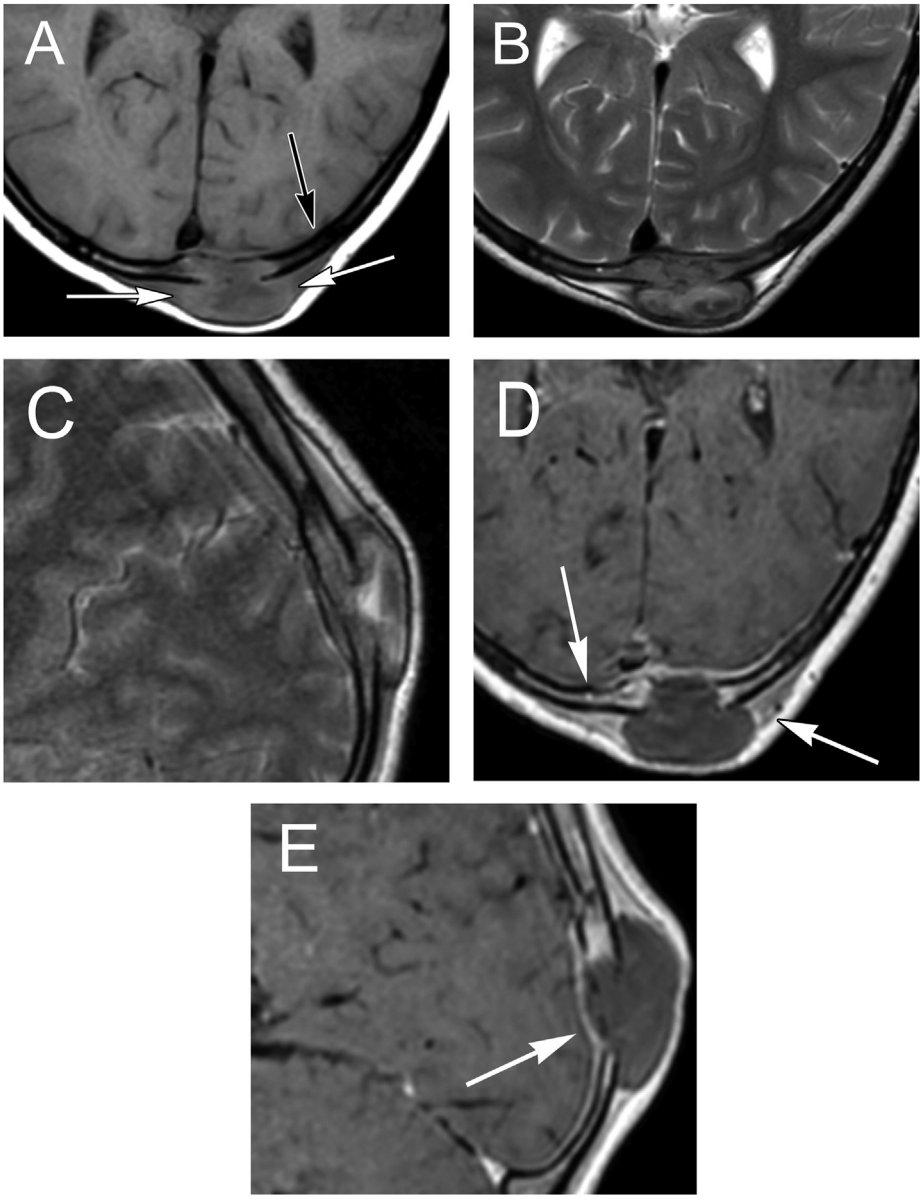

Figure 2. Single-system single-site-type occipital bone LCH of a 10-year-old boy (case 9). (A) Axial T1WI demonstrates a hyperintense mass with a bulging sign forming an eccentric portion outside the cranium. The periphery shows a hyperintense rim suggesting a penumbra sign (white arrows). Surrounding bone marrow shows hypointensity suggesting grade 2 bone marrow edema (black arrow). (B) and (C) Axial and sagittal T2WI demonstrate a heterogeneous hyperintense mass. (D) and (E) Axial and sagittal contrast-enhanced T1WI demonstrate a rim-like enhancement of the mass and enhancement of the surrounding bone and soft tissue (D: arrows). Meningeal enhancement is also seen (E: arrow). WI, weighted imaging.

informed patient consent was waived due to the retrospective nature of this study. Patient anonymity was maintained.

Forty-eight consecutive patients with a newly confirmed histopathological diagnosis of LCH anywhere in the body, based on either surgical or biopsy specimens, were retrospectively identified from the pathology database between April 2003 and May 2021. Among them, patients were included if any lesion was formed in a craniofacial bone during the disease course and if data from any contrast-enhanced MRI study were available prior to treatment. In total, 22 patients were enrolled in this study. We collected clinical data on age at presentation of the craniofacial bone lesion, sex, craniofacial bone lesion distribution, manifestation type, treatment methods, and other clinical details, including the presence of extra-craniofacial bone lesions and recurrences. Manifestation type was classified as SS-s, SS-m, or MS. We then regrouped patients with the SS-s type into the solitary lesion group (SLG) and those with the SS-m and MS types into the multiple lesions group (MLG) depending on the requirement of chemotherapy.

2.2. MRI protocol

All patients underwent MRI examinations before biopsy or surgery. Various imaging methods were used owing to the updates and changes to MR scanners and imaging protocols that occurred during the long study period of almost 18 years. All MRI examinations were performed in the axial plane for T2WI and unenhanced T1WI. Sagittal T2WI and unenhanced T1WI were performed in five and seven patients, respectively. Coronal T2WI and unenhanced T1WI were performed in two and five patients.

Fast spin echo T2WI was performed with the following parameters: repetition time (TR)/echo time (TE) range, 3283–6800/66–120 ms; field of view (FOV), 18–26 cm; slice thickness, 3.0–7.0 mm; interslice gap, 0–1.5 mm; and matrix, 198 × 288 to 420 × 512. Fast spin echo T1WI was performed using the following parameters: TR/TE range 380–2962/8.0–15 ms; FOV, 18–26 cm; slice thickness, 0.9–7.0 mm; interslice gap, 0–1.75 mm; and matrix, 192 × 240 to 392 × 512.

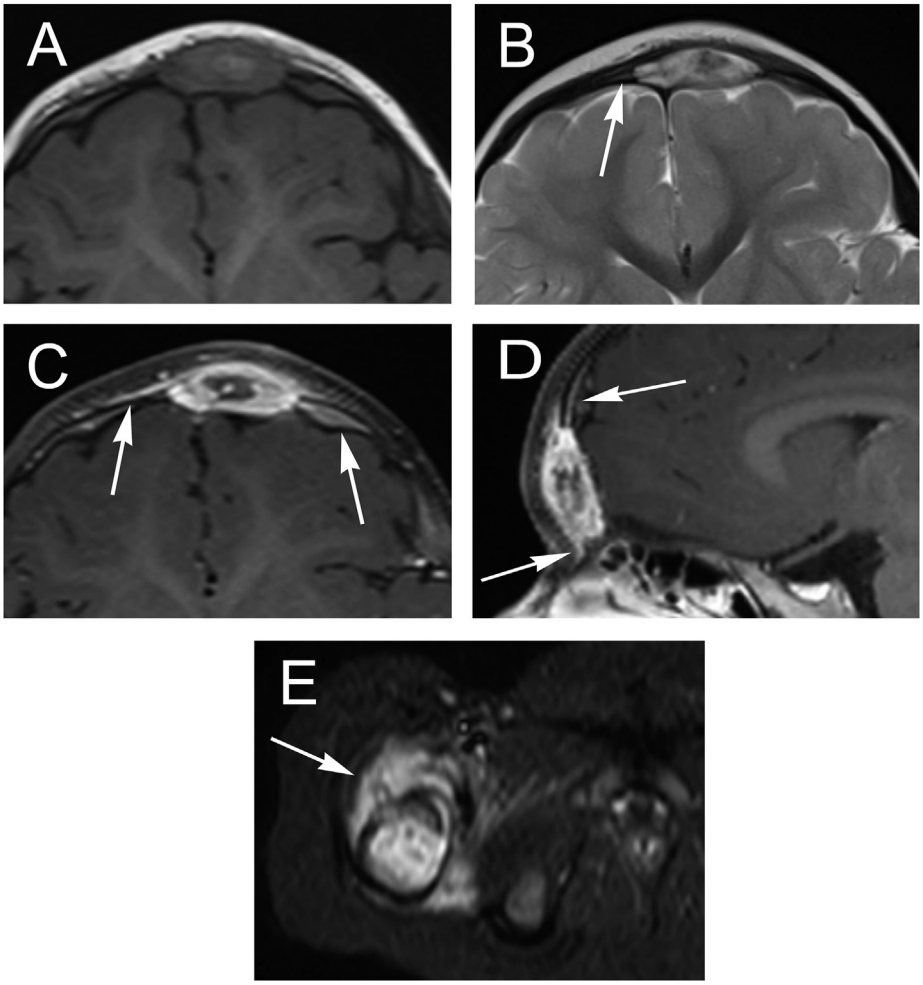

Figure 3. Single-system multifocal-site-type LCH of a 1-year-old girl (case 16). (A) Axial T1WI demonstrates a hyperintense mass in the frontal bone with a bulging sign forming a concentric soft tissue mass. (B) Axial T2WI demonstrates a hyperintense mass with grade 1 bone marrow edema (arrow). (C) and (D) Axial and sagittal contrast-enhanced T1WI with fat saturation demonstrate heterogeneous enhancement with a central unenhanced area in the mass lesion, and enhancement of the surrounding bone and soft tissue are also seen (arrows). (E) Axial short-tau inversion recovery imaging shows an infiltrative mass in the right femoral bone (arrow). WI, weighted imaging.

In all 22 patients, axial contrast-enhanced T1WI scans were obtained 3 min after intravenous injection of 0.1 mmol/kg of gadolinium-based contrast agents. Fat saturation was observed in 16 patients. Additionally, more than one plane (sagittal, coronal, or both) was obtained in all patients. Contrast-enhanced T1WI was performed using the following parameters: TR/TE range, 16–2962/6.4–20 ms; FOV, 18–26 cm; slice thickness, 0.5–7.0 mm; interslice gap, 0–1.75 mm; and matrix, 192 × 192 to 392 × 512.

2.3. Image analyses

MRI scans were retrospectively evaluated by two radiologists (with 4 and 21 years of experience, respectively) who were blinded to clinical data other than the fact that all patients had been diagnosed with LCH. Each observer individually reviewed all images with internal and surrounding details of the lesions. They evaluated signal intensity on unenhanced T1WI and T2WI scans compared to that in facial muscle, the presence and extent (partial or circumferential) of T1WI and T2WI hypointense rims, presence of a necrotic or cystic part (defined as fluid-like hyperintensity on T2WI without enhancement), fluid-fluid level (FFL, defined as different intensities being contained within a cystic or compartmentalized structure on either T1WI or T2WI), penumbra sign (rim of higher T1WI signal intensity around the lesion than in the internal part of the lesion itself), "budding" (focally invading the cortex producing a bud-like appearance) and "'bulging" (invading the adjacent two cortices) signs [9, 10], presence and distribution of extra-osseous soft tissue mass (concentric or eccentric), soft tissue edema, and bone marrow edema graded as 0–3 using the classification by James et al. (grade 0: no edema; grade 1: edema present, smaller than the lesion size; grade 2: edema present, equivalent to the lesion size; grade 3: edema present, greater than the lesion size) [11]. The enhancement pattern (homogeneous, heterogeneous, or rim-like, indicating central necrosis as described by Moon et al. [12]) and the presence of surrounding bone, soft tissue, and meningeal enhancement were evaluated on contrast-enhanced T1WI. When two or more craniofacial lesions were detected in one patient, the largest lesion was selected for evaluation of these features because some lesions were too small for precise visual assessment.

In cases of discrepancy between the observers regarding each evaluation point, the observers discussed their decisions and reached a final decision by consensus.

2.4. Statistical analyses

Statistical analyses were performed using EZR version 1.54 statistical software (Jichi Medical University, Saitama, Japan) [13]. Differences between the SLG and MLG were analyzed using Fisher's exact test for categorical variables and the Mann–Whitney U test for continuous variables. Statistical significance was set at $P < 0.05$.

Kappa analysis was used to determine the extent of agreement between the two radiologists regarding MRI evaluations. Kappa values of <0.40, 0.41–0.60, and 0.61–1.0 were considered to indicate poor, good

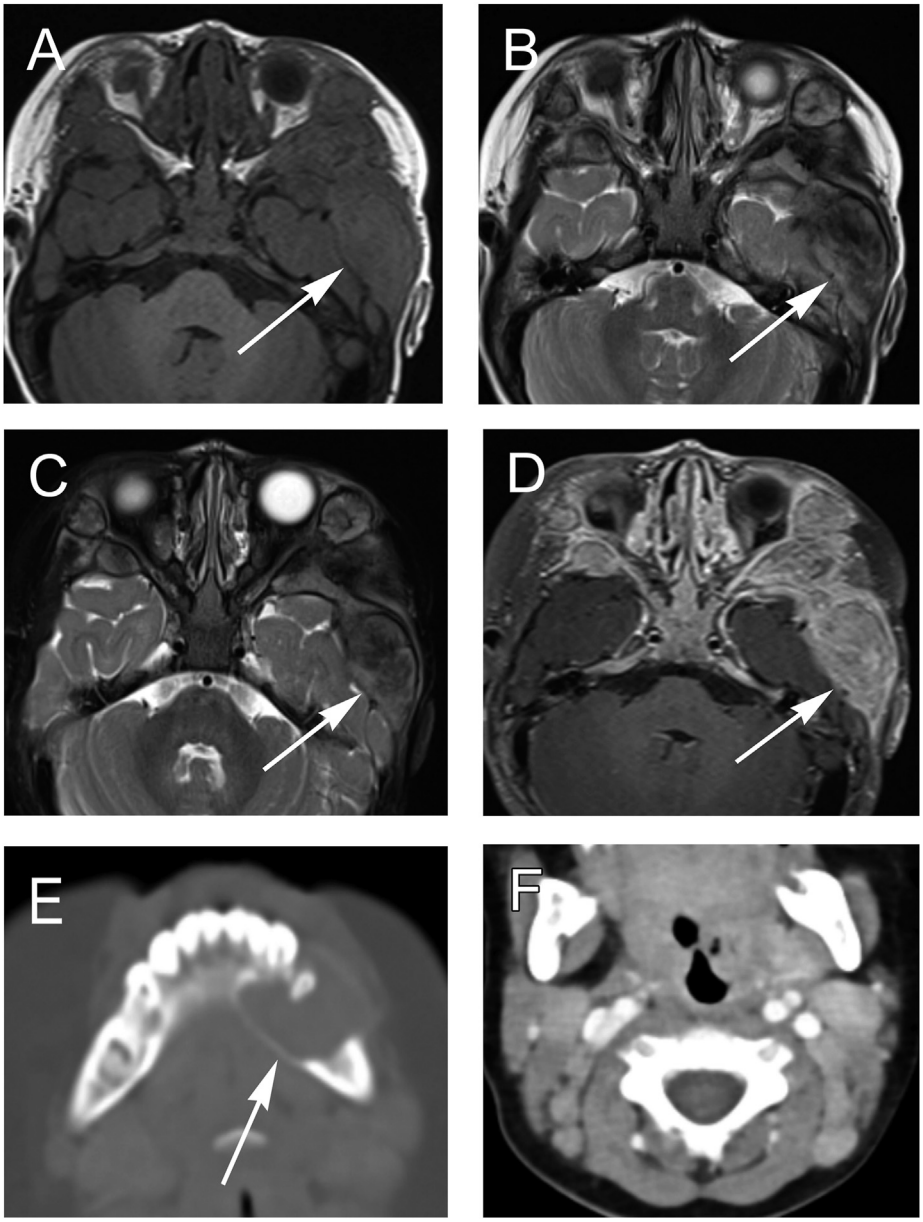

Figure 4. Multi-system-type LCH of a 2-year-old girl (case 20). (A) Axial T1WI demonstrates multiple isointense lesions in both sphenoid wings and the left temporal bone. The left temporal mass is the largest one (arrow in A, B, C, and D) and shows a bulging sign with a concentric soft tissue mass. (B) and (C) Axial T2WI with and without fat saturation demonstrate hypointense left temporal mass with slight soft tissue edema and without bone marrow edema. (D) Axial contrast-enhanced T1WI with fat saturation demonstrates heterogeneous enhancement of the mass and slight enhancement of the surrounding bone and soft tissue. (E) and (F) Axial computed tomography shows an expansile well-defined osteolytic mandibular mass lesion (E: arrow) and bilateral cervical lymph node swelling. WI, weighted imaging.

agreement, and excellent agreement, respectively, as suggested by Landis and Koch [14].

3. Results

3.1. Clinical findings

The clinical characteristics of all 22 patients are summarized in Table 1. The mean age at presentation was 5 years (range, 1–17 years), and there were 15 male patients and 7 female patients (ratio: 2.1:1). The frontal bone was the most commonly involved bone (n = 9), followed by the temporal (n = 7), occipital (n = 5), and parietal (n = 4) bones. Two cases involved the sphenoid and mandibular bones, and one case involved the zygomatic bone. Ten (45%) cases showed SS-s-type manifestation, eight (36%) cases showed SS-m-type manifestation, and four cases (18%) showed MS-type manifestation. Among the 22 patients, 10 (45%) were categorized into the SLG and 12 (55%) into the MLG. All patients with MS- and SS-m-type manifestations were treated with chemotherapy. Most patients with SS-s-type manifestation were closely monitored after excision, except for one case involving the lateral wall of the orbit, a CNS risk bone, that underwent chemotherapy.

3.2. MRI findings

Unenhanced T1WI showed hyperintensity in 15 (68%) cases and isointensity in seven (32%) cases, while T2WI showed hyperintensity in 16 (73%) cases, isointensity in three (14%) cases, and hypointensity in three (14%) cases. One (5%) case showed a circumferential hypointense rim, while the others did not show any hypointense rim. Eleven (50%) cases had necrotic or cystic parts, and five (23%) cases had FFL. Five (23%) cases showed a penumbra sign, 18 (82%) cases showed a bulging sign, and one (5%) case showed a budding sign. Seven (32%) patients had extra-osseous concentric soft tissue components, and six (27%) patients had eccentric components. Sixteen (73%) patients showed perilesional soft tissue edema. Grades 1, 2, and 3 bone marrow edema was observed in nine (41%), three (14%), and four (18%) cases, respectively.

Contrast-enhanced T1WI revealed a homogeneous enhancement pattern in nine (41%) cases, a heterogeneous pattern in 11 (50%) cases, and a rim-like pattern in two (9%) cases. Enhancement of the surrounding bone and soft tissue was identified in 17 (77%) and 16 (73%) cases, respectively. Meningeal enhancement was detected in eight (36%) cases.

3.3. Comparison of clinical and MRI findings between the SLG and the MLG

A comparison of the clinical and imaging findings between the SLG and the MLG is shown in Table 2. Among the 22 patients, 10 (45%) were categorized into the SLG and 12 (55%) into the MLG. The mean age at presentation in the SLG was significantly higher than that in the MLG (9 years vs. 2 years; $P = 0.0014$). There were eight boys and two girls in the SLG, and seven boys and five girls in the MLG, showing no significant difference between sexes.

In the SLG, unenhanced T1WI showed hyperintensity in eight (80%) cases (Figures 1A, 2A) and isointensity in two (20%) cases, while T2WI showed hyperintensity in six (60%) cases (Figures 1B, 2B, and 2C), isointensity in three (30%) cases, and hypointensity in one (10%) case. One (10%) case showed a circumferential hypointense rim, while the others did not show any hypointense rim. Six (60%) cases had necrotic or cystic parts, and four (40%) cases had FFL (Figure 1B). Four (40%) cases showed a penumbra sign (Figure 2A), eight (80%) cases showed a bulging sign (Figures 1 and 2), and one (10%) case showed a budding sign. Three (30%) cases had an extra-osseous concentric soft tissue component (Figure 1), and three (30%) cases had an eccentric component (Figure 2). Eight (80%) cases showed perilesional soft tissue edema (Figure 1C). Grades 1, 2, and 3 bone marrow edema was observed in four (40%), one (10%) and four (40%) cases, respectively (Figures 1D, 2A). Contrast-enhanced T1WI in the SLG revealed four (40%) cases with a homogeneous enhancement pattern, four (40%) cases with a heterogeneous pattern (Figures 1E, 1F), and two (20%) cases with a rim-like pattern (Figures 2D, 2E). Enhancement of the surrounding bone and soft tissue was identified in all (100%) and six (60%) cases, respectively (Figures 1E, 1F, and 2D). Meningeal enhancement was detected in five (50%) cases (Figure 2E).

In the MLG, unenhanced T1WI showed hyperintensity in seven (58%) cases (Figure 3A) and isointensity in five (42%) cases (Figure 4A), while T2WI showed hyperintensity in 10 (83%) cases (Figure 3B) and hypointensity in two (17%) cases (Figure 4B). None of the cases exhibited a hypointense rim. Five (42%) cases had necrotic or cystic parts, and one (8%) case had FFL. One (8%) case showed a penumbra sign, and 10 (83%) cases showed a bulging sign (Figures 3A–D, 4A–D). Four (33%) cases had an extra-osseous concentric soft tissue component (Figures 3A–D, 4A–D) and three (25%) cases had an eccentric component. Eight (67%) cases showed perilesional soft tissue edema (Figures 3B, 4B, and 4C). Grades 1 and 2 bone marrow edema was observed in five (42%) and two (17%) patients, respectively (Figure 3B). None of the patients showed grade 3 bone marrow edema. Contrast-enhanced T1WI in the MLG revealed five (42%) cases with a diffuse enhancement pattern and seven (58%) cases with a heterogeneous pattern (Figures 3C, 3D, and 4D). Enhancement of the surrounding bone and soft tissue was identified in seven (58%) and 10 (83%) cases, respectively (Figures 3C, 3D, and 4D). Meningeal enhancement was detected in three (25%) cases.

There were no differences in the MRI findings between the groups, except for the grade of bone marrow edema, which was significantly higher in the SLG than in the MLG ($P = 0.032$) and enhancement of the surrounding bone, which was significantly more frequent in the SLG than in the MLG ($P = 0.040$).

The kappa coefficient between the two radiologists was 0.645–1.000, indicating excellent agreement.

4. Discussion

To the best of our knowledge, this is the largest study on craniofacial bone LCH among those that have reported the number of patients who underwent contrast-enhanced MRI. In our study, the following contrast-enhanced MRI features were observed in >50% of patients: surrounding bone enhancement, surrounding soft tissue enhancement, and no meningeal enhancement. Thus, contrast-enhanced MRI revealed additional findings, mainly the surrounding details, which were clinically significant. We also compared the clinical and MRI features between the SLG and MLG based on therapeutic strategies. Among the 22 patients, 10 (45%) were classified into the SLG and 12 (55%) were classified into the MLG. In terms of clinical features, the age at presentation in the MLG (2 years) was lower than that in the SLG (9 years) ($P = 0.0014$). On MRI, perilesional bone marrow edema and enhancement were more prominent in the SLG than in the MLG ($P = 0.032$ and $P = 0.040$, respectively).

Craniofacial bone involvement in LCH is frequent, with reported frequencies varying from 54% to 73% [2, 7, 15]. The age distribution (mean age, 5 years; range, 1–17 years) in our study was similar to that in a previous study [7]. Among calvarial bones, the parietal bone is the most commonly affected bone [7]; however, the frontal bone was the most frequent site in our study. Most of the MRI findings in our study were consistent with those reported by Singh et al. [6]; however, the frequency of budding signs, bulging signs, and soft tissue mass formation were different. This may be attributed to differences between the flat and long bones. Craniofacial bones consist of flat bones that can easily form bulging signs rather than budding signs because most LCH lesions show erosion of both the inner and outer plates.

The differential diagnoses of pediatric craniofacial bone lesions include neuroblastoma metastasis, intradiploic epidermoid cyst, and fibrous dysplasia [16]. Most patients with neuroblastoma metastasis are less than 2 years old, and computed tomography typically demonstrates soft-tissue masses with lytic destruction and spiculated periosteal reaction [17]. Epidermoid cysts usually show intradiploic bone remodeling and reactive sclerotic margins, and MRI demonstrates hyperintensity on diffusion-weighted image and a low apparent diffusion coefficient value [16]. Fibrous dysplasia typically demonstrates expansile osseous remodeling with ground-glass appearance on computed tomography. The imaging findings of these differential diagnoses are considerably different from those of LCH; thus, it is easy to differentiate between LCH and these diseases. In addition, in our LCH cases, five (23%) patients showed FFL or penumbra signs, although these are not common characteristic findings compared to the imaging findings described previously. Singh et al. [6] noted that FFL and penumbra signs are rarely observed in skeletal LCH lesions. The penumbra sign is a highly specific sign of Brodie's abscess [18]. However, the penumbra sign has also been reported in cases of localized LCH, chondrosarcoma, benign cystic lesions of the bone, and intraosseous ganglion [19]. FFL in craniofacial bone LCH has been described in several studies [20, 21, 22], and Nabavizadeh et al. [22] reported LCH as the most frequent cystic bone lesions with FFL in children. Although this finding occasionally makes it difficult to differentiate LCH from aneurysmal bone cysts and cephalohematomas, perilesional bone marrow edema and enhancement can serve as clues for differentiating LCH from these differential diagnoses. Additionally, LCH lesions with FFLs are mainly reported in the craniofacial bones rather than in the appendicular bones [23, 24]. These FFLs represent hemorrhage, which can be caused by trauma or can develop spontaneously. Some LCH cases have shown pathological secondary aneurysmal bone cyst formation [25, 26]. Our study revealed that these MRI findings were not as rare as previously described; therefore, LCH should be included in differential diagnoses when craniofacial bone destructive lesions with FFL or the penumbra sign are found.

In our study, four (18%) cases showed MS-type manifestations. The prevalence of MS-type manifestation in our study was lower than that

reported in a previous large cohort study [27]. This tendency was also seen in other studies focused on bone LCH [28, 29], although the prevalence of MS-type manifestation has not been investigated among patients with craniofacial bone LCH. Kim et al. [30] reported that the bone was the most frequently affected site in their study population, although it was the second most common site in patients under 1 year of age, implicating less frequent manifestation of bone lesions in patients with MS-type manifestation.

MLG patients had a younger predominance than SLG patients. Although the classification of manifestation type differs, it is consistent with previous studies [31, 32]. Younger children have a greater risk of multi-system disease and an unfavorable clinical course. However, bone involvement is considered a favorable prognostic factor among patients with MS-type LCH, reflecting a relatively slow development of the disease [33].

In our study, 73% patients showed bone marrow edema around craniofacial bone LCH lesions. Moreover, perilesional bone marrow edema and enhancement were more extensive in the SLG than in the MLG. Based on the frequent detection of BRAF or other members of the RAS/RAF/MEK pathway mutation, LCH is thought to be an inflammatory neoplastic disorder [34]. Bone marrow edema is a frequent finding in early-stage LCH, reported in >90% of cases on MRI [9, 35]. The frequency of perilesional bone marrow enhancement has not been described in the literature; however, several previous studies have reported this feature [6, 36]. Galluzzo et al. [37] reported that pathological myelofibrosis was present in 94% patients with MS-type LCH before treatment. This may contribute to heterogeneous signal intensity on T2WI and less bone marrow edema in MS-type LCH. In our MS-type LCH cases, however, we could not confirm concomitant myelofibrosis. Thus, the reason for perilesional bone marrow edema and enhancement differences between the SLG and MLG is unclear.

Our study has several limitations. First, MRI equipment and scanning protocols varied, as the study was retrospectively performed over a prolonged period of approximately 18 years. Second, we chose the largest lesion to analyze imaging features when the patient had several lesions, which may not reflect representative imaging features.

5. Conclusions

To the best of our knowledge, this study included the largest number of patients with craniofacial bone LCH who underwent contrast-enhanced MRI and highlighted their clinical and MRI findings. Contrast-enhanced MRI showed additional significant findings of mainly the surrounding details. The solitary type of craniofacial bone LCH tended to occur in older patients and showed more extensive bone marrow edema and enhancement compared with multiple type of craniofacial bone LCH. When a craniofacial bone LCH lesion is found, these differences may help distinguish between solitary- and multiple-type LCH, which have different treatment strategies.

Declarations

Author contribution statement

Shu Matsushita: Conceived and designed the experiments; Performed the experiments; Analyzed and interpreted the data; Contributed reagents, materials, analysis tools or data; Wrote the paper.

Taro Shimono: Conceived and designed the experiments; Analyzed and interpreted the data; Contributed reagents, materials, analysis tools or data; Wrote the paper.

Tomohisa Okuma: Conceived and designed the experiments; Performed the experiments; Analyzed and interpreted the data; Contributed reagents, materials, analysis tools or data.

Takeshi Inoue: Contributed reagents, materials, analysis tools or data.

Takao Manabe: Analyzed and interpreted the data; Contributed reagents, materials, analysis tools or data.

Yukio Miki: Conceived and designed the experiments; Contributed reagents, materials, analysis tools or data; Wrote the paper.

Funding statement

This research did not receive any specific grant from funding agencies in the public, commercial, or not-for-profit sectors.

Data availability statement

The data that has been used is confidential.

Declaration of interests statement

The authors declare no conflict of interest.

Additional information

No additional information is available for this paper.

References

[1] C. Rodriguez-Galindo, C.E. Allen, Langerhans cell histiocytosis, Blood 135 (2020) 1319–1331.
[2] A. Morimoto, Y. Shioda, T. Imamura, K. Kudo, T. Kitoh, H. Kawaguchi, H. Goto, Y. Kosaka, Y. Tsunematsu, S. Imashuku, On behalf of the Japan LCH Study Group, Intensification of induction therapy and prolongation of maintenance therapy did not improve the outcome of pediatric Langerhans cell histiocytosis with single-system multifocal bone lesions: results of the Japan Langerhans cell histiocytosis Study Group-02 Protocol Study, Int. J. Hematol. 108 (2018) 192–198.
[3] N. Grois, B. Fahrner, R.J. Arceci, J.I. Henter, K. McClain, H. Lassmann, V. Nanduri, H. Prosch, D. Prayer, Histiocyte Society CNS LCH Study Group, Central nervous system disease in Langerhans cell histiocytosis, J. Pediatr. 156 (2010) 873–881.
[4] R. Haupt, M. Minkov, I. Astigarraga, E. Schäfer, V. Nanduri, R. Jubran, R.M. Egeler, G. Janka, D. Micic, C. Rodriguez-Galindo, S. van Gool, J. Visser, S. Weitzman, J. Donadieu, for the Euro Histio Network, Langerhans cell histiocytosis (LCH): guidelines for diagnosis, clinical work-up, and treatment for patients till the age of 18 years, Pediatr. Blood Cancer 60 (2013) 175–184.
[5] R. Rajakulasingam, M. Siddiqui, M. Michelagnoli, A. Saifuddin, Skeletal staging in Langerhans cell histiocytosis: a multimodality imaging review, Skeletal Radiol. 50 (2021) 1081–1093.
[6] J. Singh, R. Rajakulasingam, A. Saifuddin, Langerhans cell histiocytosis of the shoulder girdle, pelvis and extremities: a review of radiographic and MRI features in 85 cases, Skeletal Radiol. 49 (2020) 1925–1937.
[7] N. D'Ambrosio, S. Soohoo, C. Warshall, A. Johnson, S. Karimi, Craniofacial and intracranial manifestations of Langerhans cell histiocytosis: report of findings in 100 patients, AJR Am. J. Roentgenol. 191 (2008) 589–597.
[8] J. Zaveri, Q. La, G. Yarmish, J. Neuman, More than just Langerhans cell histiocytosis: a radiologic review of histiocytic disorders, Radiographics 34 (2014) 2008–2024.
[9] J. Samet, J. Weinstein, L.M. Fayad, MRI and clinical features of Langerhans cell histiocytosis (LCH) in the pelvis and extremities: can LCH really look like anything? Skeletal Radiol. 45 (2016) 607–613.
[10] Y.S. Song, I.S. Lee, J.H. Yi, K.H. Cho, D.K. Kim, J.W. Song, Radiologic findings of adult pelvis and appendicular skeletal Langerhans cell histiocytosis in nine patients, Skeletal Radiol. 40 (2011) 1421–1426.
[11] S.L.J. James, R.J. Hughes, K.E. Ali, A. Saifuddin, MRI of bone marrow oedema associated with focal bone lesions, Clin. Radiol. 61 (2006) 1003–1009.
[12] T.Y. Moon, J. Lee, I.S. Lee, K.U. Choi, J.M. Chae, J.I. Kim, S.J. Lee, MRI and histopathologic classification of Langerhans cell histiocytosis, Curr. Med. Imag. Rev. 5 (2009) 14–18.
[13] Y. Kanda, Investigation of the freely available easy-to-use software 'EZR' for medical statistics, Bone Marrow Transplant. 48 (2013) 452–458.
[14] J.R. Landis, G.G. Koch, The measurement of observer agreement for categorical data, Biometrics 33 (1977) 159–174.
[15] D. Prayer, N. Grois, H. Prosch, H. Gadner, A.J. Barkovich, MR imaging presentation of intracranial disease associated with Langerhans cell histiocytosis, AJNR Am. J. Neuroradiol. 25 (2004) 880–891.
[16] E.M. Chung, M.D. Murphey, C.S. Specht, R. Cube, J.G. Smirniotopoulos, From the archives of the AFIP: pediatric orbit tumors and tumorlike lesions: osseous lesions of the orbit, Radiographics 28 (2008) 1193–1214.
[17] F.E. Morón, M.C. Morriss, J.J. Jones, J.V. Hunter, Lumps and bumps on the head in children: use of CT and MR imaging in solving the clinical diagnostic dilemma, Radiographics 24 (2004) 1655–1674.
[18] B. McGuinness, N. Wilson, A.J. Doyle, The 'penumbra sign' on T_1-weighted MRI for differentiating musculoskeletal infection from tumour, Skeletal Radiol. 36 (2007) 417–421.
[19] A.M. Davies, R. Grimer, The penumbra sign in subacute osteomyelitis, Eur. Radiol. 15 (2005) 1268–1270.

[20] B.W. Hindman, R.D. Thomas, L.W. Young, L. Yu, Langerhans cell histiocytosis: unusual skeletal manifestations observed in thirty-four cases, Skeletal Radiol. 27 (1998) 177–181.
[21] K. Matsushita, T. Shimono, Y. Miki, Langerhans cell histiocytosis with multiple fluid-fluid levels in the parietal bone, Magn. Reson. Med. Sci. 19 (2020) 5–6.
[22] S.A. Nabavizadeh, L.T. Bilaniuk, T. Feygin, K.V. Shekdar, R.A. Zimmerman, A. Vossough, CT and MRI of pediatric skull lesions with fluid-fluid levels, AJNR Am. J. Neuroradiol. 35 (2014) 604–608.
[23] V.R. Krishna Varanasi, M.Y. Leong, A.M. Tan, W.Q. Derrick Lian, E.L.H.J. Teo, Langerhans cell histiocytosis: another cause of a fluid–fluid level within an appendicular bony lesion, BJR Case Rep. 2 (2016) 20150408.
[24] P. Lomoro, I. Simonetti, G. Vinci, V. Fichera, L. Tarotto, P. Trovato, M.S. Prevedoni Gorone, Secondary aneurysmal bone cyst in Langerhans cell histiocytosis: case report, literature review, Eur. J. Radiol. Open 6 (2019) 97–100.
[25] F. Roncaroli, A. Consales, E. Galassi, B. Bernardi, B. Valeri, Occipital aneurysmal bone cyst secondary to eosinophilic granuloma, Pediatr. Neurosurg. 35 (2001) 103–106.
[26] C. Krishnan, Langerhans cell histiocytosis masquerading as aneurysmal bone cyst, J. Clin. Oncol. 29 (2011) e688–e690.
[27] C. Rigaud, M.A. Barkaoui, C. Thomas, Y. Bertrand, A. Lambilliotte, J. Miron, N. Aladjidi, G. Plat, E. Jeziorski, C. Galambrun, L. Mansuy, P. Lutz, A. Deville, C. Armari-Alla, Y. Reguerre, S. Fraitag, A. Coulomb, V. Gandemer, N. Leboulanger, D. Moshous, K. Hoang-Xuan, A. Tazi, S. Heritier, J.F. Emile, J. Donadieu, Langerhans cell histiocytosis: therapeutic strategy and outcome in a 30-year nationwide cohort of 1478 patients under 18 years of age, Br. J. Haematol. 174 (2016) 887–898.
[28] F. Gargano, J.J. Welch, P.M. Klinge, S.R. Sullivan, H.O. Taylor, Langerhans cell histiocytosis in the pediatric population: treatment of isolated craniofacial lesions, J. Craniofac. Surg. 30 (2019) 1191–1193.
[29] I. Ghanem, V.T. Tolo, P. D'Ambra, M.H. Malogalowkin, Langerhans cell histiocytosis of bone in children and adolescents, J. Pediatr. Orthop. 23 (2003) 124–130.
[30] B.E. Kim, K.N. Koh, J.K. Suh, H.J. Im, J.S. Song, J.W. Lee, H.J. Kang, K.D. Park, H.Y. Shin, H.S. Choi, S.H. Lee, K.H. Yoo, K.W. Sung, H.H. Koo, H.L. Jung, N.G. Chung, B. Cho, H.K. Kim, C.J. Lyu, H.J. Baek, H. Kook, J.E. Park, H.J. Park, B.K. Park, E.S. Yoo, K.H. Ryu, K.S. Lee, H.S. Kim, J.M. Lee, E.S. Park, H.S. Yoon, K.C. Lee, M.J. Lee, Y.T. Lim, H.M. Kim, S.K. Park, J.A. Park, S.K. Kim, M. Park, Y.J. Lim, Y.H. Lee, J.J. Seo, on the behalf of Korea Histiocytosis Working Party, Clinical features and treatment outcomes of Langerhans cell histiocytosis: a nationwide survey from Korea histiocytosis working party, J. Pediatr. Hematol. Oncol. 36 (2014) 125–133.
[31] A. Raciborska, K. Bilska, J. Węcławek-Tompol, O. Gryniewicz-Kwiatkowska, M. Hnatko-Kołacz, J. Stefanowicz, A. Pieczonka, K. Jankowska, F. Pierelejewski, T. Ociepa, G. Sobol-Milejska, K. Muszyńska-Rosłan, O. Michoń, W. Badowska, M. Radwańska, K. Drabko, Clinical characteristics and outcome of pediatric patients diagnosed with Langerhans cell histiocytosis in pediatric hematology and oncology centers in Poland, B.M.C, Cancer 20 (2020) 874.
[32] G. Tuysuz, I. Yildiz, N. Ozdemir, I. Adaletli, S. Kurugoglu, H. Apak, S. Dervisoglu, S. Bozkurt, T. Celkan, Langerhans cell histiocytosis: single center experience of 25 years, Mediterr. J. Hematol. Infect. Dis. 11 (2019), e2019035.
[33] M. Aricò, I. Astigarraga, J. Braier, J. Donadieu, H. Gadner, E. Glogova, N. Grois, J.I. Henter, G. Janka, K.L. McClain, S. Ladisch, U. Pötschger, D. Rosso, E. Thiem, S. Weitzman, K. Windebank, M. Minkov, Lack of bone lesions at diagnosis is associated with inferior outcome in multisystem Langerhans cell histiocytosis of childhood, Br. J. Haematol. 169 (2015) 241–248.
[34] M.L. Berres, M. Merad, C.E. Allen, Progress in understanding the pathogenesis of Langerhans cell histiocytosis: back to histiocytosis X? Br. J. Haematol. 169 (2015) 3–13.
[35] S.K. Jeh, W.H. Jee, S.J. Hong, J.Y. Kim, M.S. Sung, K.N. Ryu, S.A. Im, K.A. Chun, Y.S. Lee, J.H. Cho, Extracranial skeletal Langerhans cell histiocytosis: MR imaging features according to the radiologic evolutional phases, Clin. Imag. 36 (2012) 466–471.
[36] K. Okamoto, J. Ito, T. Furusawa, K. Sakai, S. Tokiguchi, Imaging of calvarial eosinophil granuloma, Neuroradiology 41 (1999) 723–728.
[37] M.L. Galluzzo, J. Braier, S.D. Rosenzweig, M.T. Garcia de Dávila, D. Rosso, Bone marrow findings at diagnosis in patients with multisystem Langerhans cell histiocytosis, Pediatr. Dev. Pathol. 13 (2010) 101–106.